

EXPERIMENTAL INVESTIGATION OF THE INFLUENCE OF DENSITY RATIO AND VANE EXIT MACH NUMBER ON PLATFORM COOLING

H. Abdeh - G. Barigozzi – S. Ravelli – S. Rouina

Department of Engineering and Applied Sciences, University of Bergamo, Dalmine, Italy
hamed.abdeh@unibg.it, giovanna.barigozzi@unibg.it, silvia.ravelli@unibg.it,
samaneh.rouina@unibg.it

ABSTRACT

Experimental investigation and parametric analysis were carried out to evaluate the influence of coolant to mainstream density ratio (DR) and isentropic exit Mach number (Ma_{2is}) on both thermal and aerodynamic performance of a nozzle vane cascade with platform cooling through slot or discrete cylindrical holes. Measurements were carried out on a 6-vane cascade for a base case scenario, which implied high DR of 1.5, high freestream turbulence intensity of $Tu_1 = 9.5\%$ and $Ma_{2is} = 0.4$, while varying the coolant-to-mainstream mass flow rate (MFR) between 0.5% and 1.5%. The impact of reducing DR to 1.0 and increasing Ma_{2is} to 0.68 was assessed, MFR held constant. DR was varied by injecting either air/nitrogen or carbon dioxide as coolant flow, thanks to the pressure sensitive paint (PSP) technique. Lower thermal coverage derived from reduced DR whereas higher Ma_{2is} resulted in enhanced cooling effectiveness over the perforated platform.

KEYWORDS: Gas Turbine, Film Cooling, Platform, Density ratio, PSP

NOMENCLATURE

a	speed of sound	T	temperature
C	vane chord	$Tu = u'/U$	turbulence Intensity (%)
	mass fraction concentration	u, v, w	velocity Components
D	hole diameter	U	mean velocity
$DR = \rho_c/\rho_\infty$	density ratio	X, Y, Z	cascade coordinate system
H	vane height	α	hole inclination angle
$I = \rho_c U_c^2 / \rho_\infty U_\infty^2$	momentum flux ratio	β	flow angle
	intensity	δ	boundary layer thickness
L	hole length	δ^*	displacement thickness
$Ma = U/a$	Mach number	η	film cooling effectiveness
$MFR = m_c/m_\infty$	mass flow rate (%)	ν	kinematic viscosity
p	pressure	Λ_x	turbulent length scale
P	pitch	$\zeta = \frac{U_{2is}^2 - U_2^2}{\bar{U}_{2is,ms}^2}$	kinetic energy loss coefficient
$Re_c = U_c D / \nu$	coolant Reynolds number,	Superscript	
$Re_{2is} = U_{2is} C / \nu$	isentropic outlet Reynolds	'	RMS
number		-	pitch averaged
s	vane pitch		

Subscript	
ax	axial
ave	laterally-averaged
c	coolant
cl	centerline
fg	foreign gas
is	isentropic condition
ms	at midspan

1	stator inlet
2	stator exit
∞	mainstream

Abbreviations

LDV	laser doppler anemometry
PSP	pressure sensitive paint
TLC	thermochromic liquid crystals

INTRODUCTION

Turbine endwall (or platform) areas, being largely exposed directly to the hot gas discharged by the combustion chamber, are subject to the effects of thermal failure. Accordingly, highly efficient cooling schemes are badly needed to provide adequate thermal protection but the aerodynamics of the flow within the cascade passage is not helpful. On the one hand, secondary flow structures govern the coolant flow patterns (Langston, 1980; Wright et al., 2014); on the other hand, the wide range of variation in static pressure along the perforated platform, as the flow accelerates through the passage, causes large differences in the ejection rates through film cooling holes fed by a single plenum (Thole (2006)). In other words, if one considers a single supply feeding all the holes and inviscid flow through the holes, it can be shown that the same (ideal) blowing ratio will occur for each hole placed along a constant static pressure line. Indeed, state of the art cooling techniques typically include gap/purge flow and discrete film cooling so as to protect the largest portion of the front side platform. Given the complex interaction of the coolant with the highly three-dimensional flow field, both aerodynamic and thermal aspects should be taken into account in a combined analysis, as done by Nicklas and his coauthor (Kost and Nicklas (2001); Nicklas (2001)). They experimentally investigated a turbine stator with an upstream slot and 19 holes arranged in three rows in the forward section of the passage, at $Ma_{2is} = 1.0$. Measurements showed that the passage vortex is diminished in strength because of coolant ejection from both slot and holes whereas horseshoe vortex is strengthened by slot ejection, but this latter point depends on the axial displacement of the slot itself. The conceived cooling scheme was effective in the front part of the endwall but very low levels of adiabatic film cooling effectiveness (η) were detected towards the pressure side corner. Knost and Thole (2005) confirmed that the platform area near the vane pressure side remains uncooled even though a slot is located at $0.3C_{ax}$ upstream of the vane stagnation: the only way to get a more uniform tangential coverage is to place the slot $0.47C_{ax}$ further upstream (Lynch and Thole, 2008) but the coolant is less effective when it reaches the vane passage. Tao et al. (2020) have made clear that the increase in the distance between the slot and the vane leading edge causes reduced levels of laterally averaged film cooling effectiveness (η_{av}) on the endwall entrance region nevertheless η is more evenly distributed at the slot exit. The same conclusion was drawn by Muller et al. (2020), who also studied the influence of DR on η by using nitrogen ($DR = 1.0$) and carbon dioxide ($DR = 1.6$) as tracer gases. Switching to a higher DR , at engine-like conditions ($Ma_2 = 0.6$, $Tu_1 = 5\%$), led to a decline in the overall coolant coverage downstream of an upstream purge slot as the momentum flux is lowered. Still dealing with the entrance region, Ornano and Povey (2017) used infrared thermography to measure η distributions in an engine-realistic turbine endwall geometry with two rows of cylindrical holes located just upstream of the leading edge. The most relevant conclusions, for a given cooling scheme, are the following: i) there is a momentum flux ratio (I) threshold above which secondary flows are weakened or even suppressed; ii) beyond a critical I , coolant is wasted because the improvement in η is negligible in the face of increasing coolant mass flow rate.

Shifting attention to the platform cooling inside of the passage, Shiau and his coauthors addressed several topics by applying PSP. In Shiau et al. (2019), a combination between three upstream injection angles and five film-hole design patterns was experimentally tested, under fixed mainstream ($Ma_{2is} = 0.5$, $Tu_1 = 19\%$) and coolant condition ($MFR = 1\%$, $DR = 1.5$). Although each

endwall film-hole pattern was found to have its unique flow/pressure distribution, the general rule is that the thermal coverage provided by the cooling holes located upstream of the throat is heavily dependent on the capability to suppress the secondary flows. In an annular-sector cascade operated at $Ma_2 = 0.24$ and $Tu_1 = 8\%$, Shiau et al. (2016) examined the effects of MFR and DR on endwall film cooling: the cooling hole arrangement included 95 layback fan-shaped holes inside the vane passage and 46 cylindrical holes along the edges of the platform. For a given DR , higher MFR causes liftoff in the first row of cylindrical holes; on the contrary, shaped-holes, because of reduced jet momentum, ensure longer coolant traces. Whatever the MFR , the increase in DR from 1 to 1.5 resulted in higher levels of η_{av} across the whole passage, because the coolant tends to stay more attached to the surface. In the most recent work, Shiau et al. (2020) pushed the operation of the annular-sector cascade up to transonic conditions (Ma_{2is} between 0.7 and 1.0) to evaluate the influence of mainstream velocity on η , at $Tu_1 = 12\%$, for different values of MFR (from 0.5% to 1.5%) and DR (from 1.0 to 2.0). Two rows of cylindrical holes were located at $0.35C_{ax}$ and $0.68C_{ax}$. The best film coverage from the first row was obtained at MFR of 0.75% since liftoff takes place beyond this value whereas η_{av} levels provided by the second row increase with MFR , though with a leveled off trend. Increasing both DR and Ma_{2is} had a positive effect on η : in the former case the heavier coolant stays adhered to the surface; in the latter case, the larger mainstream velocity, with thinner boundary layer, promotes the jet bending toward the wall, at least where $Ma_{2is} < 1$. Yang et al. (2020) confirmed that rising Ma_2 from 0.25 to 0.7 is beneficial to endwall overall effectiveness.

This study experimentally investigates endwall thermal coverage through two different configurations including upstream slot and discrete cylindrical film cooling holes within the passage, by varying the MFR , at fixed $DR = 1.5$, $Tu_1 = 9.5\%$ and $Ma_{2is} = 0.4$. For a representative MFR held constant, the effects of reducing DR as well as increasing Ma_{2is} were assessed from both aerodynamic and thermal point of view, in order to understand the limits imposed by scaling these parameters to engine-like conditions. This is the main strength of the proposed parametric analysis.

EXPERIMENTAL SETUP

The experimental campaign was carried out at the continuous running, suction type wind tunnel for linear nozzle vane cascades shown in Fig. 1. This facility and the cascade model (Fig. 2) have been deeply described in Barigozzi et al. (2018a). Only few details are summarized here for sake of clarity. The wind tunnel test section hosts an aft loaded 6-vane cascade typical of first high-pressure turbines characterized by a pitch-to-chord ratio of 0.765 and an aspect ratio of 0.764 (Table 1). Different platform cooling schemes, both upstream and inside of the passage, can be tested thanks to a modular conception.

The wind tunnel was run in steady state conditions at high inlet turbulence intensity ($Tu_1 = 9.5\%$) and subsonic exit speed flow of Ma_{2is} equal to 0.4 and 0.68. Inlet and exit conditions were monitored at $X/C_{ax} = -1.0$ and 1.5, respectively, using a 3-hole aerodynamic probe and a set of 31 pressure taps distributed over three passages in the tangential direction. The inlet flow was also characterized in terms of velocity profile and turbulence content. Figure 3 shows the inlet boundary layer profiles measured at variable Ma_{2is} by means of a flattened pitot probe ($\delta Ma = \pm 0.01$); integral parameters, turbulence intensity and integral length scale A_x , acquired by a single wire hot wire probe, are also reported. Both cases resulted in similar velocity profiles thus suggesting that boundary layer thickness (δ) is not affected by the tested conditions: actually, Ma_1 only changes from 0.12 to 0.2. A grid formed by cylindrical rods was used to increase the inlet turbulence intensity. Turbulence decay was found to be consistent with that shown in Barigozzi et al. (2019), providing a 9.5% Tu_1 level at the leading edge plane, as verified by a 2D LDV probe (Fig. 4b). Traverses collected at variable distance from the vane leading edge are reported in Fig. 4 to check the flow quality in the entrance region. Profiles of Ma_1 and Tu_1 indicate a regular flow approaching the cascade, which is not altered by the turbulence generator located far upstream of the leading edge.

Two cooling schemes have been considered in the present investigation: i) a slot simulating the combustor to turbine interface gap; ii) CYL configuration, that makes use of 103 cylindrical holes distributed upstream and inside of the passage (see Fig. 5a and Table 2). In the former case, a $0.042C$ width slot was conceived $0.158C_{ax}$ upstream of the leading edge plane, covering three vane passages (see Fig. 2). A 9% passage height reduction takes place in front of the leading edge, as shown in Fig. 5b. A straight channel parallel to the platform surface drives the coolant from the plenum to the slot exit section (yellow section in Fig. 5b). In the latter case, cooling holes are angled at 20° to the endwall and locally aligned with the flow direction in XY plane. They are all characterized by a length-to-diameter ratio of $L/D = 29.4$ and fed by a single plenum.

Testing conditions for all cooling schemes included variations of MFR up to 1.5%, as indicated in Table 3, while using air or nitrogen ($DR=1$) and CO_2 ($DR=1.5$) as coolant. Coolant mass flow (orifice device - $\delta m_c < \pm 2.1\%$), total pressure ($\delta p = \pm 10Pa$) and temperature ($\delta T = \pm 0.5^\circ C$) inside the plenum were monitored to control the injection conditions. The coolant outflow from the holes is expected to change in terms of jet momentum within the same row and between the rows, due to variations in endwall static pressure, for each investigated combination of MFR and DR . As an example, at $MFR = 1.0\%$ and $DR = 1$, blowing ratio values in the leading edge can be as high as 2.1, reducing down to about 0.8 close to the trailing edge. For the same overall injection conditions, values of coolant Reynolds number (Re_c) roughly fall between 5300 and 6600. A reduction in blowing ratio and an increase in Re_c , by approximately 30%, are attained at $DR = 1.5$.



Fig.1. Wind tunnel.

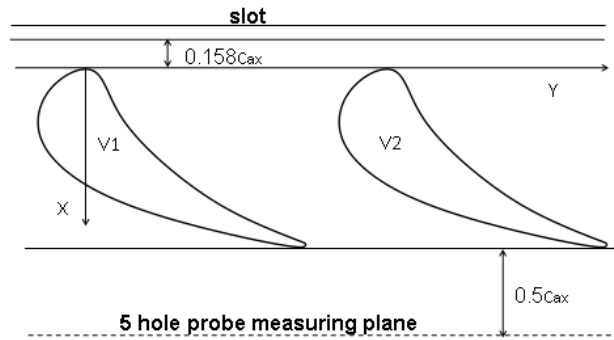


Fig.2. Nozzle vane cascade and slot.

Table 1. Cascade geometry and operating conditions

$C = 163.7 \text{ mm}$	$Ma_{2is} = 0.4 - 0.68$
$s/C = 0.765$	$Tu_1 = 9.5\%$
$H/C = 0.764$	$Re_{2is} = 1.34 \times 10^6$
$\beta_1 = 0^\circ$	$\beta_2 = 66.4^\circ$

Table 2. Hole geometry

	CYL
Nr	103
α	20°
L/D	29.4

Table 3. Test matrix

		$MFR (\%)$							
		0.5	0.7	1.0	1.5				
Ma_{2is}		DR							
		1	1.5	1	1.5	1	1.5	1	1.5
	0.4								
	0.68								

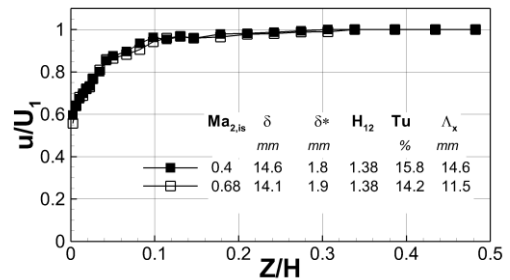


Fig. 3. Inlet boundary layer ($X/C_{ax} = -1$).

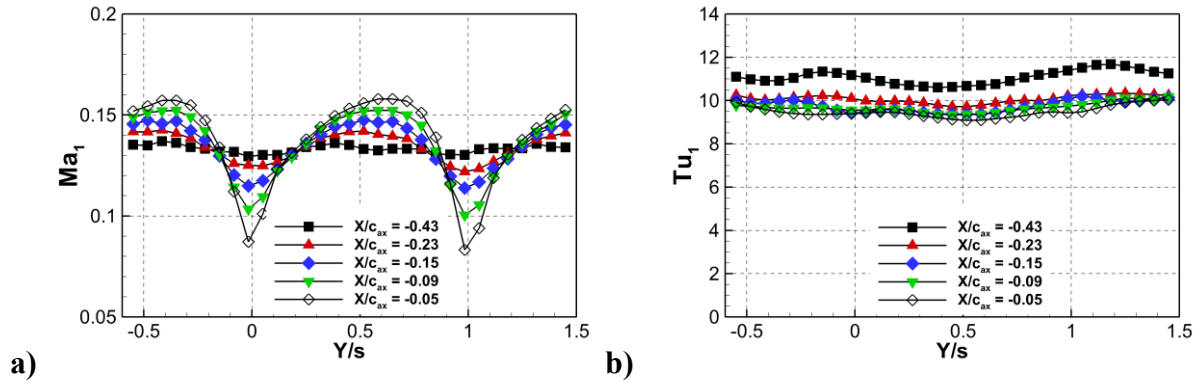


Fig. 4. Approaching flow characterization ($Ma_{2is} = 0.4$): a) Ma_1 and b) Tu_1 .

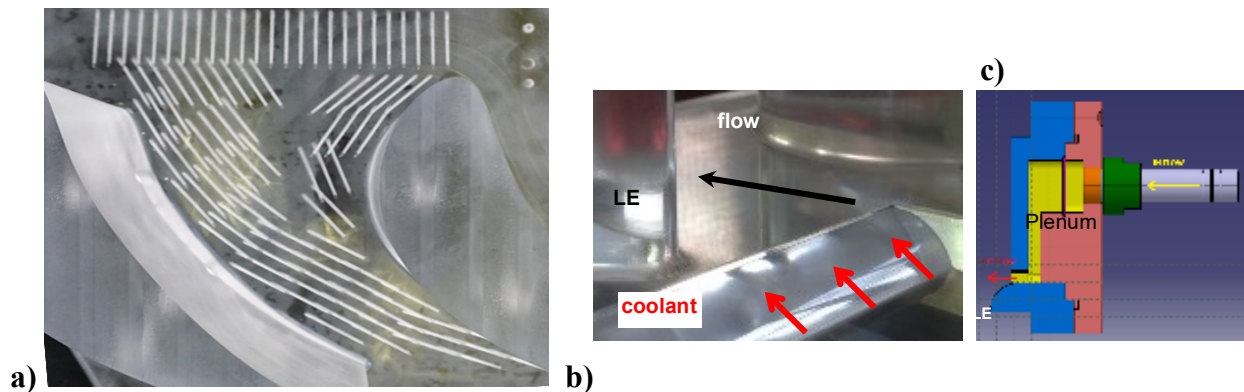


Fig. 5. Platform cooling schemes: a) CYL, b) SLOT and c) SLOT plenum.

MEASUREMENT TECHNIQUES

The impact of platform cooling on the aerodynamics of the two-dimensional cascade flow was assessed by traversing a miniaturized 5-hole aerodynamic pressure probe (2mm head diameter) at 50% of the axial chord downstream of the trailing edge plane. The probe was in-house calibrated over a wide range of Mach numbers (0.05-0.7) as well as yaw and pitch angles ($\pm 25^\circ$). Traverses extend over a single pitch, covering half of the vane span. Distributions of kinetic energy loss coefficient ($\delta\zeta = \pm 0.3\%$) were derived from local data, when injecting both air and CO_2 as coolant.

The PSP technique was used to measure η : this tool has already been successfully used at the Energy Systems and Turbomachinery laboratory - University of Bergamo - to investigate different cascade regions such as vane trailing and leading edge as well as platforms (Abdeh and Barigozzi (2018), Abdeh et al. (2020), Barigozzi et al., (2020)). As well known, the mass fraction concentration (C) of oxygen is a surrogate for temperature, as indicated in the following:

$$\eta = \frac{T_{aw} - T_\infty}{T_c - T_\infty} \approx \frac{C_{O_2,fg} - C_{O_2,\infty}}{C_{O_2,c} - C_{O_2,\infty}} = 1 - \frac{C_{O_2,fg}}{C_{O_2,\infty}} \quad (1)$$

where $CO_{2,\infty}$ is a constant value (0.231) and $CO_{2,fg}$ is the local mass fraction concentration of oxygen inside the film (Han and Rallabandi, 2010).

The binary formulation was selected in order to avoid undesirable temperature effects (Barigozzi et al. (2018)). The calibration curve (Fig. 6) was obtained in-house by changing the target surface temperature, to verify that the latter does not affect the intensity I versus pressure relationship. A stroboscopic UV lamp, a high-resolution CCD camera equipped with two sliding filters, together with a synchronization system derived from PIV are part of the setup (Fig. 7). For each testing condition, sets of 100 images were acquired injecting either N_2 or CO_2 as foreign gas,

with red and green filters to capture pressure and temperature effects. Moreover, reference (wind-off) and dark images were also collected with both filters. Images were then averaged, for noise reduction, and processed with the calibration curve (Fig. 6) to obtain the film cooling effectiveness:

$$\eta = 1 - \frac{1}{1 + \left(\frac{P_{O_2,air}/P_{O_2,ref}}{P_{O_2,CO_2}/P_{O_2,ref}} \right) \frac{MW_{CO_2}/N_2}{MW_{air}}} \quad (2)$$

The uncertainty on η value was $\delta\eta = \pm 1.4\%$ with $\eta = 0.5$ and $\delta\eta = \pm 15.6\%$ when $\eta = 0.1$.

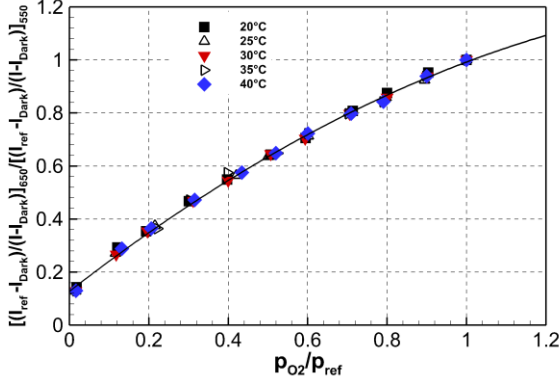


Fig. 6. Binary PSP calibration curve.

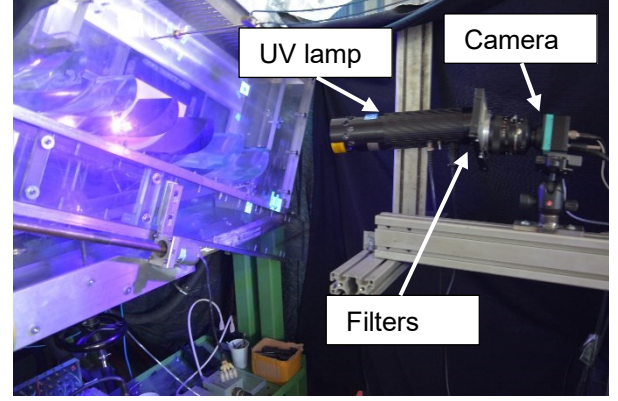


Fig. 7. PSP setup.

RESULTS

Experimental results provided information regarding the aerodynamic and thermal behavior of the considered platform cooling schemes at variable MFR , in the range between 0.5% and 1.5%. To follow, the influence of DR and Ma_{2is} on secondary flow losses and platform cooling has been discussed, taking the case at high DR , low Ma_{2is} and high Tu_1 as a reference. Please, note that measurements at $DR = 1$, both for slot and discrete holes, have already been presented in previous papers (Barigozzi et al. (2018a,2020)) and hence included in the study for comparison.

Aerodynamic aspects

Figure 8 shows the kinetic energy loss coefficient (ζ) distributions measured downstream of the trailing edge plane for the SLOT case. A single passage is reported thus including the wake behind the vane whose suction side is adjacent to the cooled channel in the case of discrete hole film cooling. Figures 7a and 7b deal with MFR variation (from 0.5% to 1.5%) at fixed cascade operating condition ($Ma_{2is} = 0.4$ and $Tu_1 = 9.5\%$), with $DR = 1.5$, whereas Figs. 8b and 8c refer to a drop in DR , from 1.5 to 1 at fixed $MFR = 1.5\%$. The typical secondary flows structure can be observed in all cases, with a well-defined loss peak at about 15% of vane span, related to the passage vortex activity, and a second loss peak close to the wall, at about 90% of the channel pitch, corresponding to the corner vortex. This pattern does not change either increasing MFR or reducing DR , consistently with a small variation in the corresponding blowing ratio, which ranges from 0.1 to 0.3. Therefore, the coolant discharged from the slot remains attached to the wall, whatever the MFR and/or DR , also thanks to the channel height reduction in front of the cascade. Hence this finding is closely related to the investigated configuration.

Shifting attention to the CYL cooling scheme, Fig. 9 displays the loss coefficient distributions measured at $DR = 1.5$, $Ma_{2is} = 0.4$ and $Tu_1 = 9.5\%$ for variable MFR values. Differently from the SLOT, the CYL cooling scheme denotes a significant impact of MFR on the aerodynamics of the cascade. It can be deduced that MFR plays a role in determining the secondary flow structure, mainly related to the jet momentum of the coolant injected in the cascade entrance region, upstream of the 3D separation line. Indeed, low injection rates are associated with secondary flow intensification, since cooling jets may interact with the generation of horseshoe and passage vortex.

On the opposite, high momentum jets reenergize the approaching boundary layer thus diminishing the losses in the passage vortex core region. This is especially evident at the highest MFR of 1.5%. The same trend was observed at lower DR (Barigozzi et al. (2018a)). As an example, results at $DR = 1.0$ are depicted in Fig. 10a, for $MFR = 1.0\%$, with the aim of combining a significant injection flow rate with passage vortex core still present. Since lowering the DR at constant MFR translates into increased cooling jet momentum, a deformation in the passage vortex losses seems to take place in Fig. 10a, in comparison with Fig. 9c, at almost comparable loss peak (about 19.5%). Finally, Fig. 10b shows ζ distribution measured at $MFR = 1.0\%$ and $DR = 1.5$, at higher Ma_{2is} of 0.68. An increase in Ma_{2is} from 0.4 to 0.68 (see Fig. 10b vs. Fig.9c) is responsible for a slight drop in the dissipation within the passage vortex core. Moreover, that core moves closer to the wall. Indeed, these findings also pertain to a solid vane cascade, when Ma_{2is} rises under subsonic flow conditions (Perdichizzi, (1989)).

To better quantify the impact of the above-mentioned parameters on loss generation, values of mass averaged overall kinetic energy loss coefficient were computed from local distributions (Fig. 11). Each value is referred to the solid configuration, i.e. the same vane cascade without any platform cooling. As expected, SLOT injection has a marginal effect on loss generation inside the passage, showing only a slight increase in loss when a very small amount of carbon dioxide is injected, i.e. a very low momentum fluid.

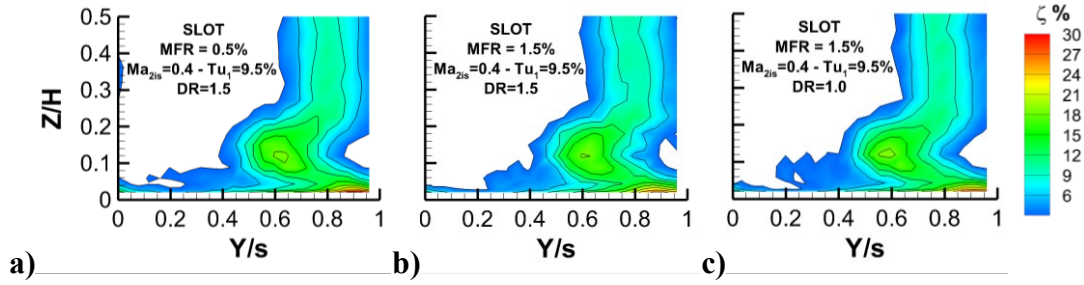


Fig. 8. SLOT kinetic energy loss coefficient distributions.

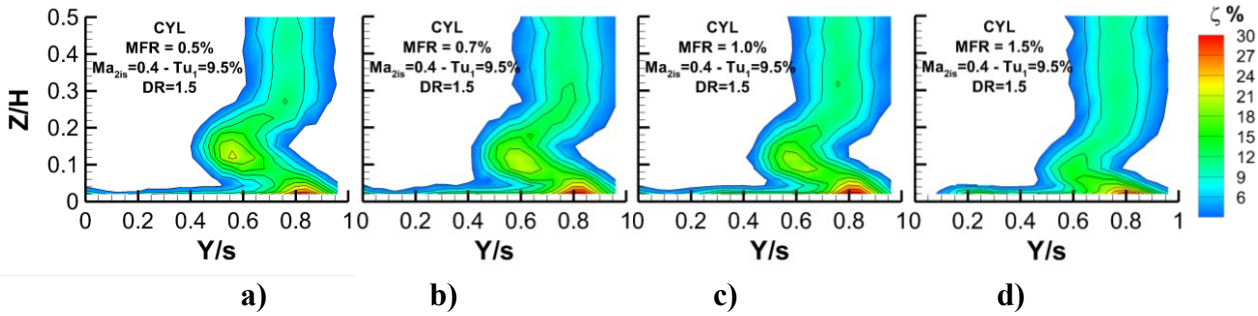


Fig. 9. CYL case kinetic energy loss coefficient distributions for variable MFR .

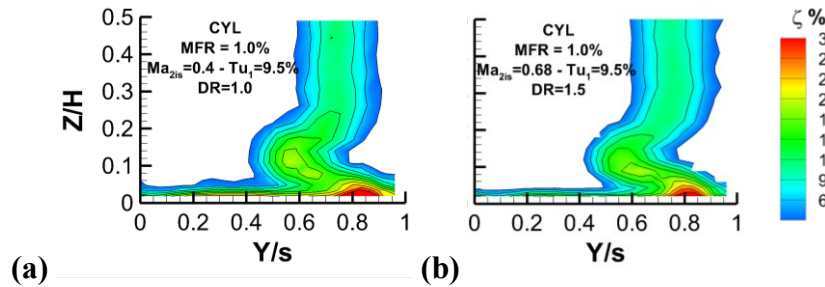


Fig. 10. CYL case kinetic energy loss coefficient distributions at $MFR=1\%$ for a) $DR=1$, b) $Ma_{2is}=0.68$.

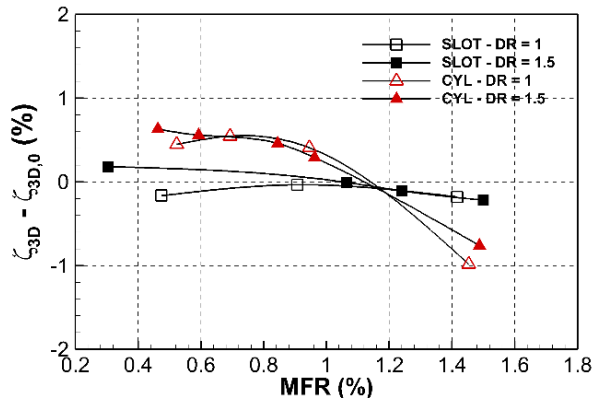


Fig. 11. Overall kinetic energy

Thermal aspects

The thermal behavior of both platform cooling schemes was investigated by means of the PSP technique. Figures 12 and 13 show contour plots of η distribution downstream of the SLOT whereas Figs. 14 and 15 report maps of η for the CYL case.

Starting from the slot case, Fig. 12 shows η contour plots at high DR , high Tu_1 , constant Ma_{2is} equal to 0.4, for variable MFR . The film cooled area is generally characterized by a triangular shape, in between the separation lines of the pressure and the suction side legs of the horseshoe vortex. Improved platform thermal protection can be achieved when rising MFR : with a low MFR of 0.5% (Fig. 12a) coolant is concentrated in the middle of the passage thus leaving both pressure and suction side of the channel uncooled. A MFR value of 1.0% (Fig. 12b) delivers a quite effective thermal coverage inside of the passage, upstream of the endwall boundary layer separation lines. However, the region surrounding the vanes and extending along the pressure and the front suction side is uncooled. A further MFR increase up to 1.5% (Fig. 12c) still ensures some benefits: effectiveness is slightly enhanced all over the protected surface but the rear pressure side region remains exposed to hot gas due to the crossflow.

At this latter MFR of 1.5%, which provides the best cooling performance, a parametric analysis was conceived consistently with the previous section (Fig. 13). A reduction in DR (Fig. 13a) causes a relevant change in the tangential extension of the coolant trace on the platform inside of the passage: in fact, coolant appears more concentrated in the middle of the passage compared to Fig. 12c. This might be due to the horseshoe vortex branches keeping the coolant farther from the vane surface, because of its higher momentum. It is fair to point out that the results reported in Fig. 13a derive exceptionally from a different measurement technique and data processing. In fact, thermochromic liquid crystals (TLC) were used in the low DR case, due to limitations in the nitrogen storage capacity. In particular, wide banded TLC and steady state approach were used (Barigozzi et al. (2020)): $\delta\eta$ varied between $\pm 4.2\%$, when $\eta = 0.8$, and $\pm 15\%$ when $\eta = 0.1$. This could partially motivate the observed differences. Conversely, the increase in Ma_{2is} (Fig. 13b) resulted in negligible modifications of the coolant footprint on the platform compared with Fig. 12c.

Now considering the CYL cooling scheme, contour plots of Fig. 14 are useful to discuss the MFR influence on η at fixed cascade operating conditions, using CO_2 as coolant ($DR = 1.5$). Figure 15 refers to $MFR = 1.0\%$ for the sensitivity analysis based on changing DR and Ma_{2is} . Increasing the MFR from 0.5% to 0.7% results in η augmentation inside of the channel but shrinking of the coolant traces is evident just downstream of the 1st row, thus suggesting jet detachment. A further increase in MFR up to 1.0% has detrimental effects on η in the entrance region, due to jet liftoff in the 1st row. The documented behavior with the difference between cooling hole rows at different axial location is in line with Shiau et al. (2020). The comparison of Fig. 15a with Fig. 14c puts in evidence that higher DR is beneficial to platform cooling since jets are allowed to stay close to the wall thanks to the reduced momentum. This is true inside of the passage but not in the entrance

region, where blowing ratios of 1st row-jets are too high even in the high DR case, so that jet detachment cannot be avoided. Increasing Ma_{2is} (see Fig. 14c vs. Fig. 15b) results in higher η levels over most of the passage: the higher flow acceleration pushes the jets close to the wall even in the channel entrance region. In this case, differently from Shiau et al. (2020), the inlet boundary layer thickness does not make any difference (see Fig. 3).

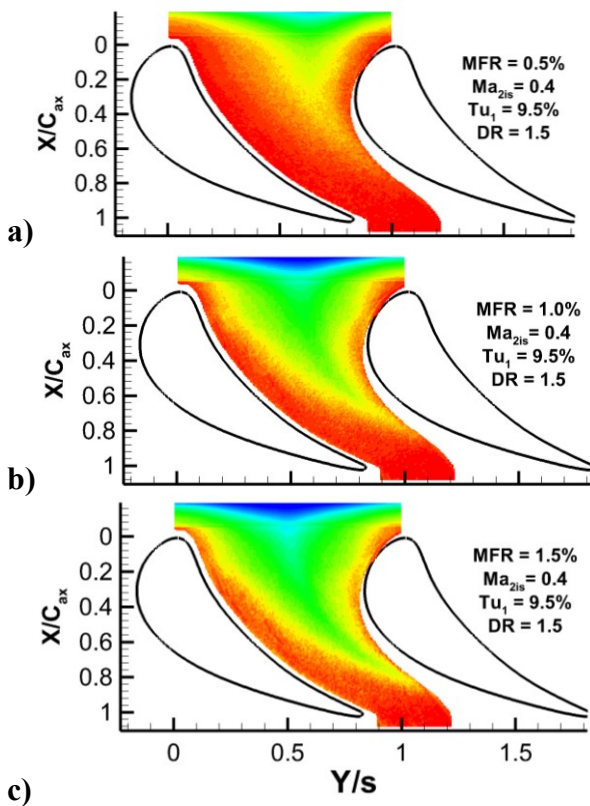


Fig. 12. Slot η contours for variable MFR ($Ma_{2is}=0.4$, $Tu_1=9.5\%$, $DR=1.5$).

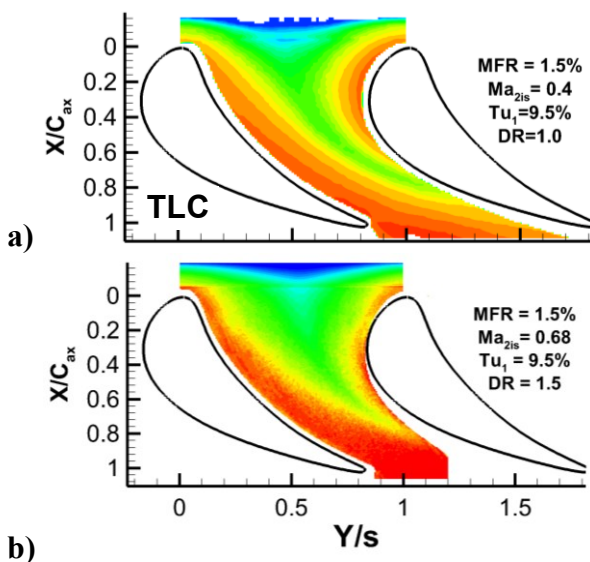


Fig. 13. Slot η contours at $MFR=1.5\%$.

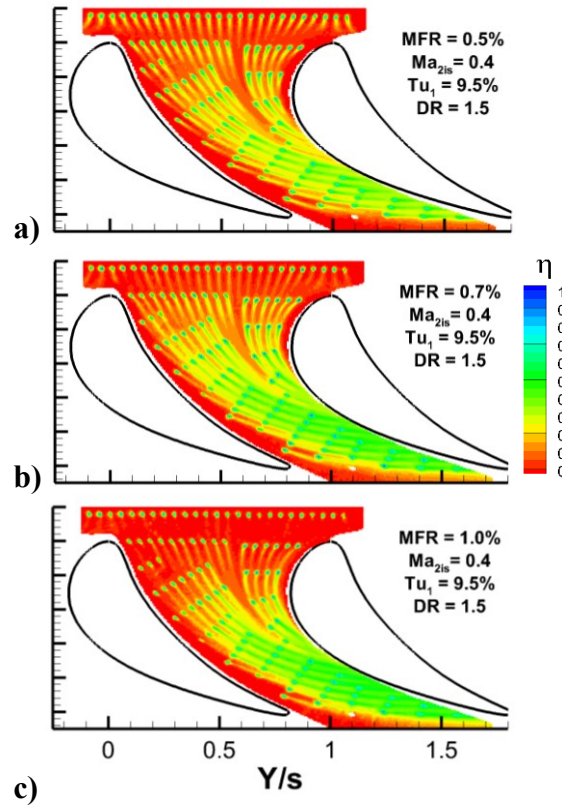


Fig. 14. CYL η contours for variable MFR ($Ma_{2is}=0.4$, $Tu_1=9.5\%$, $DR=1.5$).

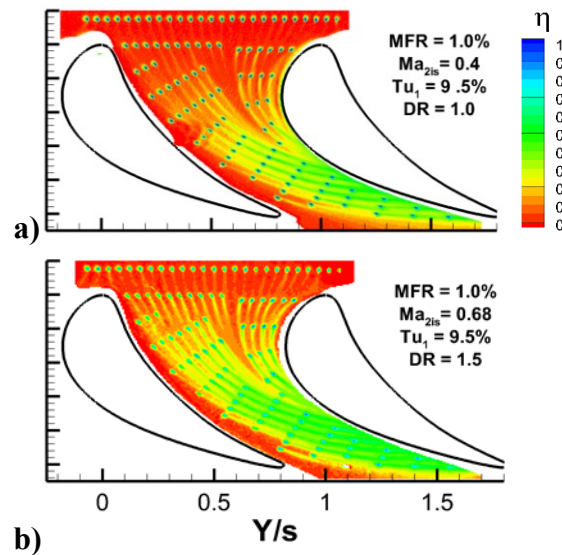


Fig. 15. CYL η contours at $MFR=1.0\%$.

To deepen the parametric analysis from a quantitative point of view, η distributions were averaged in the tangential direction. The calculated values are reported as a function of the normalized axial coordinate (X/C_{ax}): Figs. 16 and 18 focus on variable MFR for SLOT and CYL

configurations, respectively, whereas Figs. 17 and 19 highlight the effects of changing DR and Ma_{2is} on η_{av} , at a fixed MFR . Profiles of η_{av} are displaced within $X/C_{ax} \leq 0.8$ for the SLOT case because measured data are not available over the whole passage tangential extension further downstream.

Drawing attention to the SLOT, a decline in η_{av} is evident at increasing axial position, whatever the blowing condition (Fig. 16). This is typical of purge flow, as testified by Muller et al. (2020) and Tao et al. (2020). The present configuration ensures very poor thermal coverage at the rear of the passage, with $\eta_{av} < 0.2$ at $X/C_{ax} > 0.6$. An upward shift in η_{av} profile occurs due to the increase in MFR from 0.5% to 1.5% with an increment step value of 0.5%. It is evident that the improvement in η_{av} is more significant when rising MFR from 0.5% to 1.0% as compared with that obtained from the next increment of MFR , thus indicating a certain level of coolant efficiency saturation.

Figure 17 demonstrates that the influence of Ma_{2is} on η_{av} , at constant MFR of 1.5%, is marginal, whatever X/C_{ax} . Conversely, a reduction in DR gives rise to a steeper decay of η_{av} curve upstream of the throat, within $0 < X/C_{ax} < 0.6$, whereas slightly larger η_{av} values can be found at $X/C_{ax} > 0.6$, compared to the reference case (filled circles). However, this latter finding may depend on the measurement technique capability to capture the deterioration of the coolant coverage approaching the end of the passage. Moreover, overlapping η_{av} profiles at $X/C_{ax} < 0$ reveal that the slot is a robust solution: it can deliver η_{av} as high as 0.8, whatever the DR , when operated closely to coolant efficiency saturation in the entrance region.

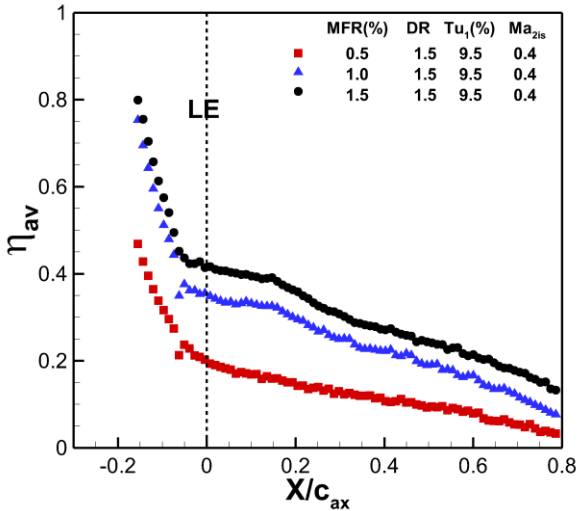


Fig. 16. Laterally-averaged effectiveness for variable MFR - SLOT.

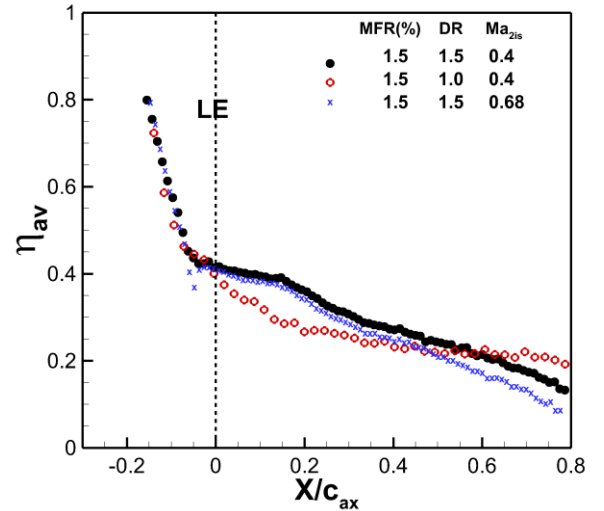


Fig. 17. Laterally-averaged effectiveness at $MFR=1.5\%$ - SLOT.

A more complex behavior characterizes the CYL cooling scheme. As a general comment, η_{av} follows an increasing trend throughout most of the passage, reaches a peak that does not exceed 0.45 at a far downstream axial position and drops to a very low level (below 0.2) downstream of the trailing edge (Fig. 18). When considering the influence of MFR on η_{av} in the reference condition, the platform can be divided into the following sections: the entrance region ($X/C_{ax} < 0$), where any increment in MFR from the lowest value of 0.5% is detrimental to cooling effectiveness; the front region ($0 < X/C_{ax} < 0.5$) where rising MFR from 0.5% to 0.7% results in η_{av} increase but further MFR augmentations cause the worst cooling performance due to jet liftoff; the rear of the passage, i.e. approximately downstream of the throat, where increasing MFR always results in a beneficial effect, though less and less substantial. At high DR , low Ma_{2is} and high Tu_1 the trade-off between higher film cooling effectiveness all over the platform versus lower coolant usage is ensured by MFR equal to 0.7%, similarly to the low DR case.

At a fixed MFR of 1.0%, Fig. 19 shows that reducing DR does not help enhancing the platform cooling: a decrease in η_{av} is documented at $X/C_{ax} > 0.3$, where higher momentum modifies the fluid dynamics of the fully attached jets whereas negligible variations in η_{av} can be seen in the upstream

region, where jet detachment is the dominant feature, whatever the DR . Higher η_{av} values are observed within $X/C_{ax} < 0.6$ when Ma_{2is} is increased, though below the subsonic flow conditions. It might be assumed that the mainstream flow, having higher velocity and acceleration, exerts a bending action on the cooling jets, in agreement with the findings reported by Yang et al. (2020).

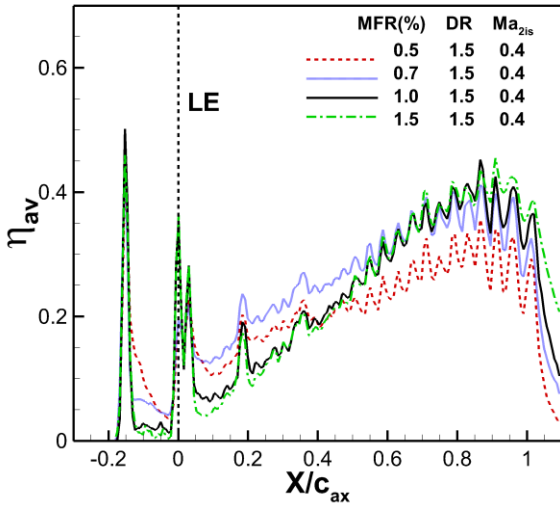


Fig 18. Laterally-averaged effectiveness for variable MFR – CYL.

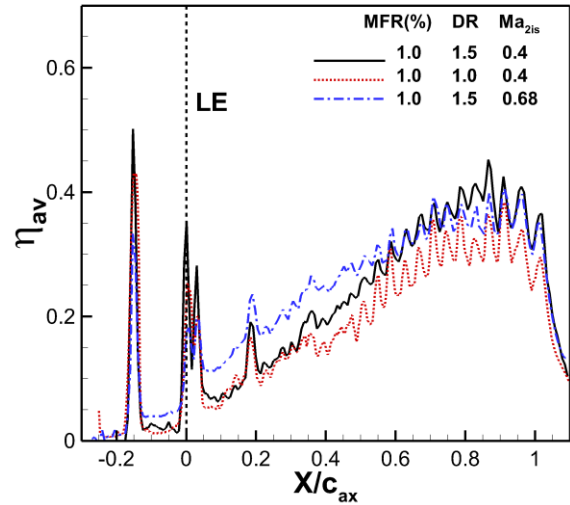


Fig 19 Laterally-averaged effectiveness at $MFR=1.5\%$ - CYL.

CONCLUSIONS

Aerodynamic and thermal measurements were executed in a linear nozzle vane cascade at engine-realistic conditions ($DR = 1.5$, $Tu_1 = 9.5\%$, $Ma_{2is} = 0.4$) to assess the performance of two platform cooling schemes, such as upstream slot and discrete cylindrical film cooling holes, at various MFR values between 0.5% and 1.5%. A parametric analysis on the effect of lower DR and higher Ma_{2is} was also carried out, at MFR held constant. The key highlights of the present study are the following:

- in the investigated MFR range, increasing the coolant flow rate is beneficial to the platform cooling obtained from slot ejection, with no increment in overall kinetic energy loss compared to the solid vane;

- in the case of cylindrical holes fed by a single plenum, each row has its specific behavior and the first one, being located upstream of the leading edge, is more at risk of liftoff. The most effective film coverage over the whole platform is provided by MFR equal 0.7%, whatever the DR value, with a rising then decreasing trend in η_{av} at increasing axial coordinate. The price to pay is increased losses (+0.5%) compared to the uncooled case.

- a reduction in DR is always detrimental to η : the lighter coolant has higher momentum thus promoting jet detachment. This is especially crucial for the CYL configuration, in which, at least, a slight reduction in kinetic losses can be gained, whatever the MFR .

- increasing Ma_{2is} helps the coolant to stay adherent to the surface, so its positive effects become significant in the CYL case, where liftoff and kinetic losses are mitigated.

- when testing a platform cooling scheme featuring cylindrical holes, it is mandatory to replicate as close as possible the engine DR and MFR . Lowering Ma_{2is} does not change the coolant-to-mainstream general behavior for variable MFR . The only effect is small overestimation of aerodynamic losses, on the one side, and underestimation of platform thermal protection, on the other side.

- conversely, endwall cooling through a slot is poorly affected by the reduction in DR and Ma_{2is} , from both aerodynamic and thermal point of view.

Indeed, the optimum solution should include both the slot and the cooling holes to maximize the area-averaged cooling effectiveness over the whole platform, under the constraints of *MFR* and aerodynamic losses. In this regard, fan-shaped holes, with low requirement of cooling air and fewer number of holes, might represent an improvement on the current arrangement, despite the increased manufacturing cost.

REFERENCES

- Abdeh, H., Barigozzi, G., (2018). *A parametric investigation of vane pressure side cutback film cooling by dual luminophor PSP*. Int J Heat Fluid Flow, 69:106-116.
- Abdeh, H., Barigozzi, G., Ravelli, S., and Rouina, S., (2020). *A Parametric Investigation of Vane Showerhead Film Cooling by Pressure-Sensitive Paint Technique*. J. Turbomach. 142(3):031007 (9 pages).
- Barigozzi, G., Mosconi, S., Perdichizzi, A., Abba, L., et al., (2018a). *Aerodynamic and Heat Transfer Experimental Investigation of Platform Cooling on a HP Nozzle Vane Cascade*. Proceedings of the ASME Turbo Expo 2018: Turbomachinery Technical Conference and Exposition, Oslo, Norway.
- Barigozzi, G., Mucignat, C., Abdeh, H., Scandella, D., et al., (2018b). *Assessment of binary PSP technique for film cooling effectiveness measurement on nozzle vane cascade with cutback trailing edge*. Exp Therm Fluid Sci, 97:431-443.
- Barigozzi, G., Perdichizzi A., Abba L., Pestelli L., (2020), *Platform Film Cooling Investigation On An Hp Nozzle Vane Cascade With Discrete Shaped Holes And Slot Film Cooling*. Proceedings of the ASME Turbo Expo 2020: Turbomachinery Technical Conference and Exposition, Virtual.
- Barigozzi, G., Perdichizzi, A., Pestelli, L., Abram, R., (2019). *Combined Experimental and Numerical Investigation of the Aero-Thermal Performance of a Rotor Blade Cascade with Platform Cooling*. Proceedings of the ASME Turbo Expo 2019: Turbomachinery Technical Conference and Exposition, Phoenix, Arizona, USA.
- Han J.C., Rallabandi A., (2010). *Turbine blade film cooling using PSP technique*. Front. Heat Mass Transf. 1(1): 1-21.
- Knost, D. G., Thole, K. A., (2005). *Adiabatic Effectiveness Measurements of Endwall Film-Cooling for a First-Stage Vane*. ASME. J. Turbomach. 127(2): 297–305.
- Kost, F., Nicklas, M., (2001). *Film-Cooled Turbine Endwall in a Transonic Flow Field: Part I- Aerodynamic Measurements*. ASME. J. Turbomach. 123(4): 709–719.
- Langston, L. S., (1980). *Crossflows in a Turbine Cascade Passage*. ASME. J. Eng. Power, 102(4): 866–874.
- Lynch, S. P., Thole, K. A., (2008). *The Effect of Combustor-Turbine Interface Gap Leakage on the Endwall Heat Transfer for a Nozzle Guide Vane*. ASME. J. Turbomach. 130(4): 041019.
- Müller, G., Landfester, C., Böhle, M., Krewinkel, R., (2020). *Turbine Vane Endwall Film Cooling Effectiveness of Different Purge Slot Configurations in a Linear Cascade*. ASME. J. Turbomach., 142(3): 031008.
- Nicklas, M., (2001). *Film-Cooled Turbine Endwall in a Transonic Flow Field: Part II—Heat Transfer and Film-Cooling Effectiveness*. ASME. J. Turbomach. 123(4): 720–729.
- Ornano, F., Povey, T., (2017). *Experimental and computational study of the effect of momentum-flux ratio on high-pressure nozzle guide vane endwall cooling systems*. ASME. J. Turbomach., 139(12): 121002.
- Perdichizzi, A., (1989). *Mach Number Effects on Secondary Flow Development Downstream of a Turbine Cascade*. Proceedings of the ASME 1989 International Gas Turbine and Aeroengine Congress and Exposition, Toronto, Ontario, Canada.
- Shiau, C., Chen, A. F., Han, J., Azad, et al., (2016). *Full-Scale Turbine Vane Endwall Film-Cooling Effectiveness Distribution Using Pressure-Sensitive Paint Technique*. ASME. J. Turbomach., 138(5): 051002.

Shiau, C., Sahin, I., Ullah, I., Han, et al., (2020). *Transonic Turbine Vane Endwall Film Cooling Using the Pressure-Sensitive Paint Measurement Technique*. ASME. J. Turbomach. 142(8): 081004.

Shiau, C., Sahin, I., Wang, N., Han, et al., (2019). *Turbine Vane Endwall Film Cooling Comparison from Five Film-Hole Design Patterns and Three Upstream Injection Angles*. ASME. J. Thermal Sci. Eng. Appl., 11(3): 031012.

Tao, Z., Yao, Y., Zhu, P., Song, L., et al., (2020). *Experimental and numerical study on film cooling effectiveness of an annular cascade endwall with different slot configuration*. Int. J. Therm. Sci., 158: 106517.

Thole, K., (2006), *Airfoil endwall heat transfer*. The Gas Turbine Handbook, NETL, 353-363.

Wright, L. M., Malak, M. F., Crites, D. C., Morris, M. C., et al., (2014). *Review of platform cooling technology for high pressure turbine blades*. Proceedings of the ASME Turbo Expo 2014: Turbine Technical Conference and Exposition, Düsseldorf, Germany.

Yang, X., Liu, Z., Zhao, Q., Liu, et al., (2020). *Comparisons of Endwall Overall Effectiveness From Two Film Hole Distribution Patterns at Low and High Exit Mach Numbers*. ASME. J. Turbomach. 142(10): 101007.